Ihnatiuk, Daryna; Tossi, Camilla; Tittonen, Ilkka; Linnik, Oksana

Effect of Synthesis Conditions of Nitrogen and Platinum Co-Doped Titania Films on the Photocatalytic Performance under Simulated Solar Light

Published in:
Catalysts

DOI:
10.3390/catal10091074

Published: 17/09/2020

Document Version
Publisher's PDF, also known as Version of record

catalysts

MDPI

Article

Effect of Synthesis Conditions of Nitrogen and Platinum Co-Doped Titania Films on the Photocatalytic Performance under Simulated Solar Light

Daryna Ihnatiuk [1,2], Camilla Tossi [1], Ilkka Tittonen [1] and Oksana Linnik [3,*]

[1] Micro and Quantum Systems Group, Department of Electronics and Nanoengineering, Aalto-University, Tietotie, 3, 02150 Espoo, Finland; dar_ign@ukr.net (D.I.); camilla.tossi@aalto.fi (C.T.); ilkka.tittonen@aalto.fi (I.T.)

[2] Hydrometallurgy and Urban Mining Group, School of Engineering Science, Lappeenranta-Lahti University of Technology, Yliopistonkatu, 34, 53850 Lappeenranta, Finland

[3] Chuiko Institute of Surface Chemistry of the NAS of Ukraine, General Naumov Str., 17, 03680 Kyiv, Ukraine

* Correspondence: okslinnik@yahoo.co.uk; Tel.: +38-044-422-96-98

Received: 27 July 2020; Accepted: 15 September 2020; Published: 17 September 2020

Abstract: Platinum and nitrogen co-doped titania films of different surface morphologies obtained via a sol-gel process have been tested for tetracycline hydrochloride photocatalytic decomposition under simulated solar light. Titania crystallization to anatase is shown by XRD for all films. A shift of the bandgap edge toward the visible region in absorption spectra and, consequently, a narrowing of the bandgap is observed for some films doped with nitrogen and/or exposed to UV pretreatment. The surface peculiarities of the samples are presented by an SEM and TEM investigation. The surface saturation by Pt and N with a homogeneous distribution of Pt ions on the surface as well as bulk as established by XPS and EDS data can be achieved with a certain synthesis procedure. The influence of the platinum content and of the pretreatment procedure on the state and atomic surface concentration of incorporated nitrogen and platinum is studied by XPS analysis: substitutional and interstitial nitrogen, non-metal containing fragments, Pt^0, Pt^{2+} and Pt^{4+} ions. The photocatalytic activity of the films is ruled by the presence of Pt^{2+} ions and N rather than Pt^0. The formation of the polycrystalline titania structure and Pt^0 nanoparticles (NPs) is confirmed by TEM and electron diffraction images. The mechanism of primary photocatalytic processes is proposed.

Keywords: photocatalysis; sol-gel; titania; platinum; nitrogen; XPS; nanoparticles

1. Introduction

The growing scientific and technological interest in the construction of new composite materials with unique properties is directed by their applications as sensors, photocatalysts, catalysts and optical issues [1–3]. Environmental photocatalysis is one of the recently developing advanced treatment approaches for the removal of anthropogenic chemicals, which appeared as a result of the accelerated development of industrial and manufacturing rates during the last century [4].

The attempts of various TiO_2 modifications in order to manipulate its electronic structure and adjust its absorption to lower energy light have been widely reported [5]. Exposure to visible light, efficient photogenerated charge separation through the narrowing of the material's bandgap, or the formation of additional sublevels within the bandgap were studied and still remain the main goal of titania modification [6]. Numerous synthesis approaches have been reported for the manufacturing of active doped titania using single or double doping [6–9]. Depending on the nature and the

concentration of the doping agents, they can act either as charge traps or as recombination sites. To prompt the photocatalytic reaction, the trapped charges have to interact with the pollutant species on/near the surface of a photocatalyst; therefore, an extensive investigation of the surface peculiarities of semiconductive materials is a determinative issue in photocatalysis [10,11].

Nitrogen-doped TiO_2 is intensively studied as a prospective catalytic material under visible irradiation [12–17]. Different aspects of nitrogen incorporation have a considerable effect on the surface properties of the material and can be analyzed through X-ray photoelectron spectroscopy (XPS): the states (substitutional and/or interstitial) of doped nitrogen, the formation of new bonds, the atomic content of each element and their oxidation states. The interpretation of N1s peak position and N contribution in the mechanism of the photocatalytic process are still under debate [18–21]. The substitutional and interstitial states of nitrogen are reported [13,22,23] to be responsible for the activity under UV and visible light due to the hybridization of the N 2p and O 2p orbitals, leading to a cathodic shift of the valence band energy or to the formation of additional energy sublevels within the bandgap.

Titania modification by metals or p-type semiconductors leads to the formation of a high enough Schottky barrier or p–n junction, respectively, both of which provide a barrier that rectifies the charge transfer and, as a result, an efficient charge separation [24,25]. Therefore, a modification with noble metals positively also affects the photocatalytic activity of TiO_2 [26]. It is also noticeable that the concentration of noble metals, particularly Pt, in nanocomposites should increase until the optimum point (up to 1–2 mol.%), otherwise, dopant species start acting as the recombination sites or shield titania from incoming light [27]. Several techniques for integrating platinum as a dopant in nanostructured semiconductors have been studied, such as sol-gel, impregnation, physical mixing and photodeposition, with the aim of controlling the morphology, the load and the oxidation state of the metal [28–32]. The oxidation state of Pt species in Pt-doped TiO_2 is shown to affect the photocatalytic degradation of chlorinated organic compounds, with the photocatalytic activity increasing in the order TiO_2 < TiO_2/oxidized Pt species < TiO_2/metallic Pt [33]. Based on a photoelectrochemical investigation, the generation of the photocurrent is increased in a Pt^0/TiO_2 electrode, compared to the oxidized Pt species, which act as recombination centers in titania. Titania co-doping by N and Pt is shown [34] to increase the activity under UV–vis irradiations in nearly six times compared to Degussa P25 as a result of multivalent states of platinum in conjunction with N.

Features of the sol-gel synthesis of semiconductive films based on titania allow the creation of structures with different morphologies on various substrates [10,35]. As known, photocatalytic reactions occur on the interface of solid photocatalysts and the liquid or gas phase where the adsorption of reactant molecules or ions is one of the determining factors of an efficient photocatalytic transformation [10]. The sol-gel method is the simplest and a cost-effective technique for the manufacturing of thin films. It allows the synthesis of films with controllable morphologies, high homogeneity and easier applicability in the photocatalytic processes by means of exclusion of the energy consuming extraction of powder from the liquid phase.

In this study, the correlation between the sol-gel synthesis conditions, optical, structural, and surface properties of films based on titania co-doped with N and Pt and their photocatalytic activity in tetracycline hydrochloride (TC) degradation is reported. An analysis of experimental results reveals the key points for the design and synthesis of new photocatalytic systems. UV pretreatment and/or co-doping TiO_2 at certain sol-gel conditions by urea and Pt(II) acetylacetonate are responsible for the formation of the different Pt species and their ratios as well as the substitutional and interstitial nitrogen incorporation in titania. Such composite materials can be applied as the catalysts not only for various photocatalytic processes (photosplitting of water, H_2 production, etc.) but also for catalytic and electrochemical demands.

2. Results

Platinum and nitrogen co-doped titania films of different morphologies (Figure 1) have been synthesized by the sol-gel method. Platinum (II) acetylacetonate has been used as a precursor of doped

2. Results

Platinum and nitrogen co-doped titania films of different morphologies (Figure 1) have been synthesized by the sol-gel method. Platinum (II) acetylacetonate has been used as a precursor of doped metal ions, especially, of divalent Pt ions accessible for both oxidation and reduction processes and yet acetylacetonate counter-ions could be easily inbuilt into the organic sol framework during the synthesis. The photocatalytic destruction of TC molecules over the films has been carried out to investigate the influence of the surface morphology, chemical composition and nitrogen doping on their photocatalytic efficiency. For this purpose, some different approaches have been used: (i) the different synthesis routes to obtain different surface morphologies and (ii) UV treatment of the intermediate layers of the films to produce Pt^0 nanoparticles (NPs). An addition of Pluronic 123 as a template and acetylacetone as a stabilizing agent provides the formation of a porous structure that is conserved after sintering at 450 °C (Method 1). The smoothed and non-porous surface is observable for films obtained using the other simpler route (Method 2). SEM images of 1Pt,N-TiO_{2M1} and 1Pt,N-TiO_{2M2} films are presented in Figure 1.

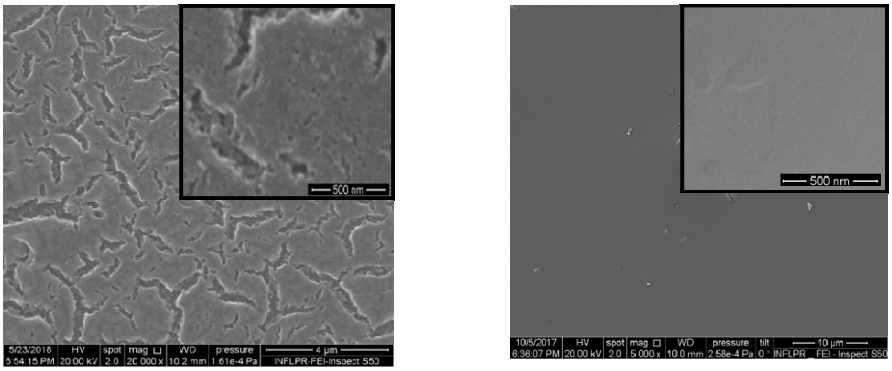

(**a**) (**b**)

Figure 1. SEM images: (**a**) 1Pt,N-TiO_{2M1} film; (**b**) 1Pt,N-TiO_{2M2} (b) film.

The optical behavior of 1 mol.% Pt-doped films obtained by Method 1 and Method 2 (Figure 2) is critically different. The shift of the absorption band edges to a shorter wavelength than in pure titania film can be caused by the Q-size effect, i.e., the formation of lower particle sizes (Figure 2a). However, the absorption intensity in the range of 350–450 nm increases for 1Pt-TiO_{2M1}, 1Pt,N-TiO_{2M1} and 1PtN-TiO_{2M1UV}, which can be a result of the formation of intra bandgap states, due to the presence of dopants' ions in the electronic structure of the semiconductor [27] and can be partially due also to localized surface plasmon resonance in the Pt nanoparticles embedded in the TiO_2 [36]. The similar spectral character has been noted for the films containing 0.5 mol.% of Pt ions (Figure S1a). The films obtained by Method 2 exhibit a high intensity in the visible part of the spectrum (the color of the films were muddy yellow) indicating the different ability to absorb and scatter light that can be connected to the structural features of the materials (Figure 2b). Optical spectra of the films containing 0.5 mol.% of Pt ions showed a much lower intensity in the visible region (Figure S1b) compared to the films with 1 mol.% Pt. As shown by the XPS data presented below, the atomic content of Pt species on the surface of 1Pt,(N)-TiO_{2M2} films exceeds the one of 1Pt,(N)-TiO_{2M1} resulting in not only high intensity of absorption but also light scattering. It is assumed that the formed Pt^0 NPs are accumulated over the film surface leading to a significant contribution in light scattering that is clearly seen in the case of 1Pt,N-TiO_{2M2UV} and 0.5Pt,N-TiO_{2M2UV} (curve 5 in Figure 2b and and Figure S1b).

The emission spectrum of the irradiated source (Figure S1c) shows that the excitation of the semiconductor materials takes place in the spectral region of sunlight. The intensity of the lamp without and with a cut-off filter (0–360 nm; 700–1200 nm) and the wavelength of the daily sunlight were measured by a pyroelectric wattmeter VP-1 in the middle of May (50.474084° N, 30.343643° E).

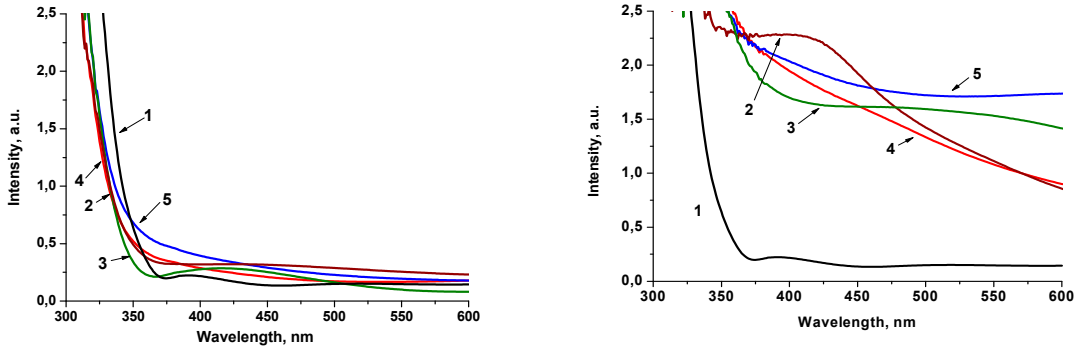

Figure 2. Absorption spectra of 1 mol.% Pt-doped films prepared by Method 1 (**a**) and Method 2 (**b**): (1) TiO_2; (2) Pt-TiO_2; (3) Pt-TiO_{2UV}; (4) Pt,N-TiO_2; (5) Pt,N-TiO_{2UV}.

The indirect transition bandgap energy values (E_{bg}) of the films of Method 1 obtained under different conditions are found to be within 3.5–3.7 eV, while the films of Method 2 are characterized by a lowered E_{bg}, in particular for 1Pt-TiO_{2UV}, 1Pt,N-TiO_2 and 1Pt,N-TiO_{2UV} (Table 1). TiO_2 and N-TiO_2 films are characterized by 3.7 and 3.8 eV, respectively, for Method 1 and 3.6 eV for Method 2 (Figure S2). The variation of optical E_{bg} values is suggested to be connected to the size of TiO_2 particles formed at the presented synthesis conditions as a result of a different aggregation degree [11] and/or hydrolysis rate of titanium tetraisopropoxide during sol formation.

Table 1. Bandgap energy values of titania for indirect transition obtained from absorption spectra.

Film	*Method 1*	*Method 2*
	E_{bg}, eV	
TiO_2	3.7	3.6
N-TiO_2	3.8	3.6
0.5Pt-TiO_2	3.5	3.6
0.5Pt-TiO_{2UV}	3.7	3.4
0.5Pt,N-TiO_2	3.5	3.4
0.5Pt,N-TiO_{2UV}	3.5	3.4
1Pt-TiO_2	3.5	3.5
1Pt-TiO_{2UV}	3.5	3.3
1Pt,N-TiO_2	3.6	3.3
1Pt,N-TiO_{2UV}	3.6	3.2

Crystallization of titania to anatase occurs for all samples after heating at 450 °C (Figure 3). The 2θ anatase peaks corresponding to about 25.4° (101), 38.9° (004), 48.1° (200), 54.1° (105), 54.9° (211), 62.4° (204) and 69.0° (213) (JCPDS 21-1272) are observed, as shown in Figure 3. The XRD peaks at 31.8° and 45.6° marked by stars in the Figure 3 do not correspond to any crystalline form of titania and platinum oxide and are related to the trace of impurities of unknown nature that require detailed investigation. The N-TiO_2 films of Method 1 and Method 2 contain anatase and the mixture of anatase and brookite, respectively (Figure S3).

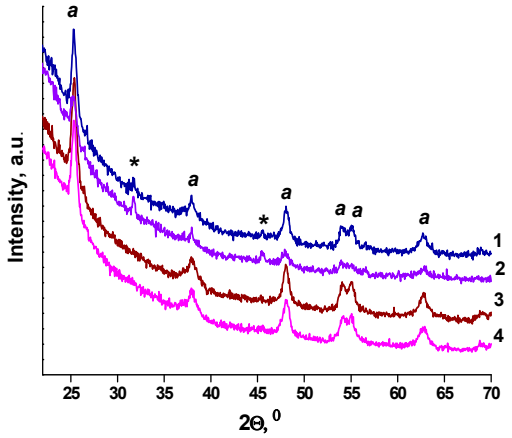

Figure 3. XRD patterns of the films (a-anatase): (1) 1Pt-TiO_{2M1}; (2) 1Pt,N-TiO_{2M1}; (3) 1Pt-TiO_{2M2}; (4) 1Pt,N-TiO_{2M2}.

An XPS analysis was applied to clarify the effect of different synthesis conditions on the composition of the surface layer: (i) different valence states of platinum; (ii) doping efficiency of both Pt and N. Atomic ratios of the elements on the surface obtained by the XPS data showed that the surface of the films of Method 12 contained less Pt and N compared to Method 2 (Table 2). The surface of the films of Method 2 is more enriched by Pt and N compared to Method 1. Analyzing the elements' ratio on the surface and bulk of 1Pt-TiO_2 and 1Pt,N-TiO_2, it can be summarized that Pt is more homogeneously distributed in the structures obtained by Method 2. The ratio of Ti and O approached the stoichiometric value for both surface and bulk.

Table 2. Atomic ratios of the elements on the surface (XPS) and bulk (EDS data of some films are presented in brackets).

Film	Pt	N	Ti:	O	Pt	N	Ti	O
	Method 1				*Method 2*			
0.5Pt-TiO_2	0.004	-	1.000	2.285	0.006	-	1.000	2.248
0.5Pt,N-TiO_2	0.004	0.017	1.000	2.288	0.004	0.032	1.000	2.163
0.5Pt-TiO_{2UV}	0.003	-	1.000	2.868	0.006	-	1.000	2.463
0.5Pt,N-TiO_{2UV}	0.001	0.004	1.000	3.264	0.006	0.028	1.000	2.207
1Pt-TiO_2	0.004	-	1.000	2.401	0.013	-	1.000	2.149
(EDS)	*(0.016)*	-	*(1.000)*	*(1.645)*	*(0.011)*	-	*(1.000)*	*(2.116)*
1Pt,N-TiO_2	0.005	0.009	1.000	2.357	0.011	0.043	1.000	2.085
(EDS)	*(0.011)*	-	*(1.000)*	*(1.932)*	*(0.014)*	-	*(1.000)*	*(1.871)*
1Pt-TiO_{2UV}	0.010	-	1.000	2.321	0.015	-	1.000	2.230
1Pt,N-TiO_{2UV}	0.005	0.027	1.000	3.239	0.010	0.12	1.000	2.680

The maxima of $Ti2p_{3/2}$ XPS peaks (Figure 4 and Figure S4) are centered at 458.5–458.7 eV, with a spin-orbit split component equal to 5.7 eV, corresponding to the Ti^{4+} atom surrounded by oxygen atoms. The slight shift to a lower binding energy (BE) (0.2 eV) of $Ti2p_{3/2}$ maxima observed for nitrogen-doped films (Method 1) can be caused by nitrogen incorporation in the titania matrix in the form of substitutional and interstitial atoms (Table 3). The O1s line showed the peaks corresponding to O^{2-} and surface OH groups, at binding energy (BE) values near 530 and 531 eV (Figures S4 and S5).

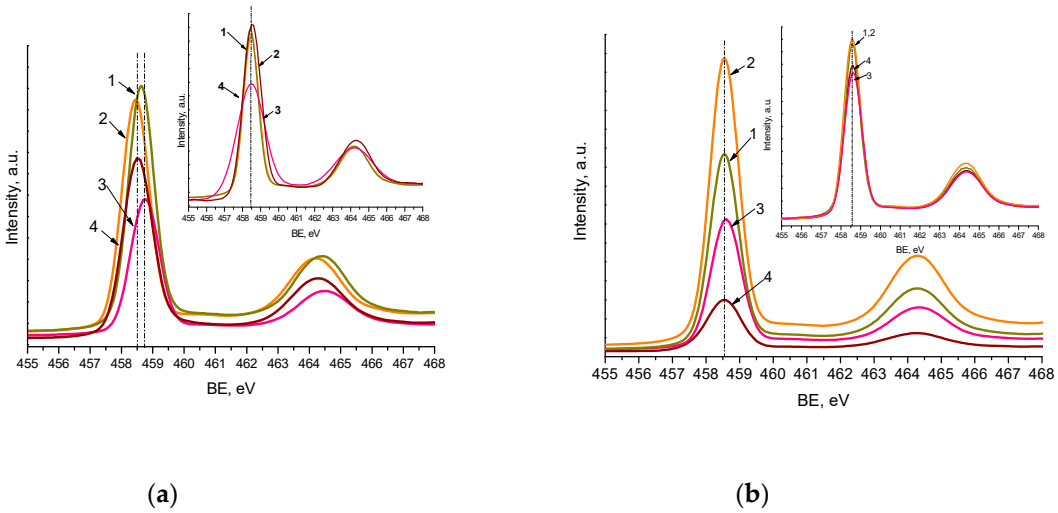

(**a**) (**b**)

Figure 4. Ti2p XPS spectra of the films synthesized by Method 1 (**a**) and Method 2 (**b**) contained 1 mol.% Pt and 0.5 mol.% Pt (insert): Pt-TiO_2 (1), Pt,N-TiO_2 (2), Pt-TiO_{2UV} (3), Pt,N-TiO_{2UV} (4).

Nitrogen incorporation in the Pt,N-TiO_2 structure takes place in its various states as it is evident from N1s XPS lines (Table 3, Figure 5) compared to N-TiO_2 (Figure S4). The most prominent line at BE = 399.8 ± 0.2 eV, observed for all N modified films, overlaps with the value assigned to the nitrogen-containing organic compounds that originated from the pyrolysis products of urea and corresponds to C-N-C fragments [37–39]. The maxima at higher BEs (400.5–404.1 eV) belong to the nitrogen surrounding at least one element more electronegative than carbon, corresponding to the O–N–Xbonds, where Xis C or O. The N1s peak at 398.0 ± 0.3 eV is also found in some cases and can be assigned to the formation of Ti-O-N fragments [40].

Table 3. Binding energy values of N1s peaks and their relative intensity (I_{rel}).

BE, eV Film	395.8 ± 0.2	397.1	398.0 ± 0.3	399.8 ± 0.2	400.5–404.1
			I_{rel}, %		
0.5Pt,N-TiO_{2M1}	-	-	4.8	81.7	13.5
0.5Pt,N-TiO_{2M1UV}	-	-	-	85.3	14.7
1Pt,N-TiO_{2M1}	3.5	-	-	74.2	22.3
1Pt,N-TiO_{2M1UV}	-	8.1	-	81.8	9.4
0.5Pt,N-TiO_{2M2}	-	-	3.5	76.8	19.7
0.5Pt,N-TiO_{2M2UV}	-	-	-	67.6	32.4
1Pt,N-TiO_{2M2}	1.9	-	6.1	84.9	7.0
1Pt,N-TiO_{2M2UV}	-	-	8.3	66.2	25.5

Lower BE values fixed at 395.8 ± 0.2 and 397.1 eV characterize the formation of common bonds between Ti and N (Ti-N) defined as substitutional (N*s*) and interstitial (N*i*) atoms, respectively [20,41,42]. The relative intensity of N*s* and N*i* to other N states is still low and found only for the samples containing 1 mol.% Pt. It has to be pointed out that nitrogen incorporation in the N*s* form (BE~396 eV) is only reported for a few instances of nitrogen and metal ions co-modified, titania obtained by the sol-gel method (using urea and $RuCl_3$ [39], ammonia and $Sr(NO_3)_2$ [43], dodecylamine and $Fe(NO_3)_3 \bullet 9H_2O$ [44], tetramethylethylenediamide and Pt^0/Pt^{2+} [45]). Additionally, N1s lines with BE at 397.5 defined by XPS in the samples obtained by the solvothermal method using urea and H_2PtCl_6 are also reported [46]. Thus, the possibility of N to be incorporated in N*s* and N*i* forms by means of the sol-gel technique depends on the nature of the co-doped metal ions.

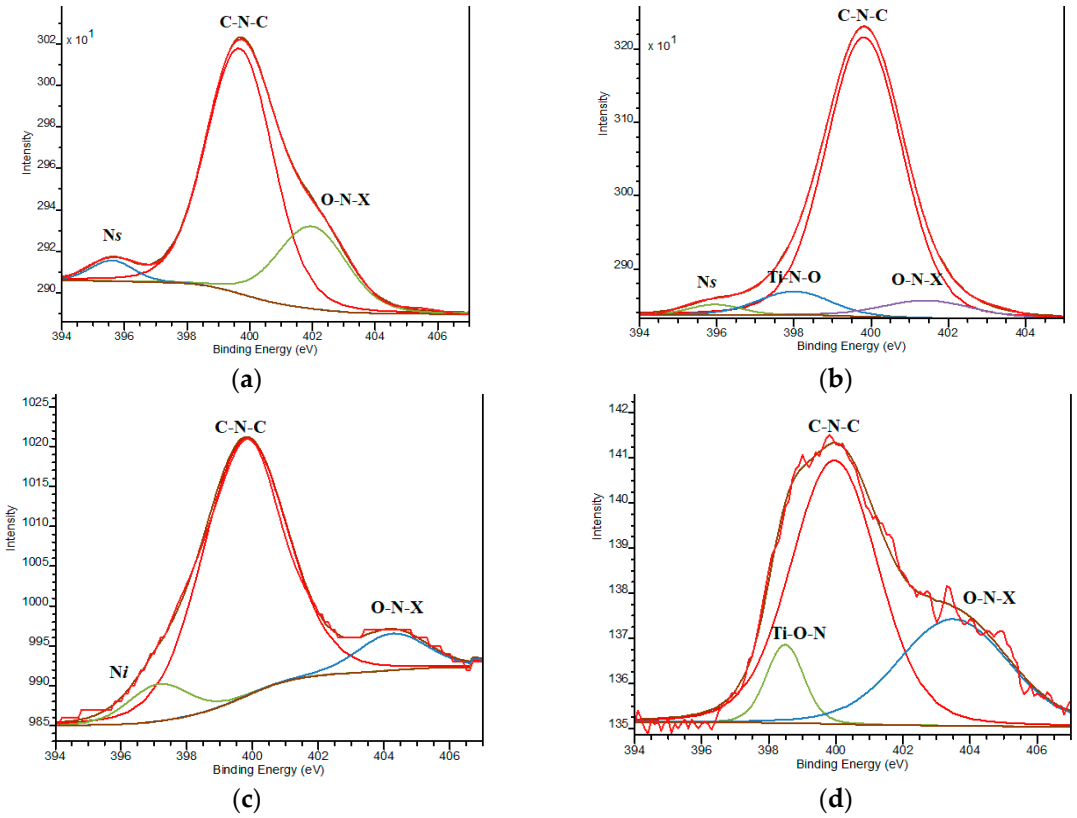

Figure 5. XPS N1s deconvoluted lines: (**a**) 1Pt,N-TiO_{2M1}; (**b**) 1Pt,N-TiO_{2M2}; (**c**) 1Pt,N-TiO_{2M1UV}; (**d**) 1Pt,N-TiO_{2M2UV}.

As reported in [47–49], the metal ions related to hard Lewis acids (Ti is among them) are bonded to urea via an oxygen atom while the soft Lewis acids (including Pt) form the monodentate ligand via the metal–nitrogen bond and sometimes via the metal–oxygen one (Scheme 1a,b). Taking into account that the titanium-containing sol is acidified to control the hydrolysis rate, the protonation of urea molecules can occur via oxygen atoms preventing Ti^{4+}–urea complexation while the interaction via N of the amide group with Pt^{2+} can still take place (Scheme 1c). As a result, urea thermolysis can happen not only through a polycondensation reaction with the formation of heterocyclic compounds [50] defined in N1s at 399.8 ± 0.2 eV (Table 3), but also via the urea decomposition resulting in the formation of reactive nitrogen species (ammonia, cyanic acid) [6] due to its complexation to Pt^{2+} ions, leading to the formation of N*s* and N*i* atoms.

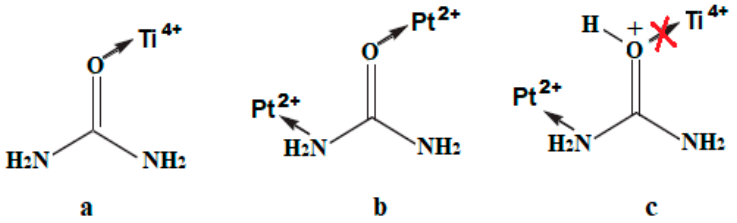

Scheme 1. Possible pathways for urea molecule complexation with metal ions: (**a**) Ti^{4+}; (**b**) Pt^{2+}; (**c**) Ti^{4+} and Pt^{2+} in acidified sol.

The XPS spectra of Pt4f lines exhibit complex non-symmetric shaped curves, indicating the presence of various Pt oxidation states (Figure 6 and Table 4). A spin-orbit coupling is established according to the position of the energy of deconvoluted Pt4f lines, in the range of 3.3–3.4 eV (Table S1), with the intensity ratio of $Pt4f_{7/2}$:$Pt4f_{5/2}$ = 4:3. Since the area of the $Pt4f_{5/2}$ region exceeded the $Pt4f_{7/2}$ one, the deconvolution was performed considering the overlapped peak of Al2p (BE values of Al^{3+} are

situated at 74.6–75.6 eV) [51] (Figure 7). The presence of Al^{3+} ions can be explained by the traces of this element from the reagents used in the synthesis procedure.

Reduction of Pt^{2+} to Pt^0 is confirmed by XPS lines with BE at 69.6–71.4 eV (Figures 6 and 7 and Table 4) and EDS mapping images (Figure 8). The large gap in these values can be explained by the different sizes of Pt nanoparticles (NPs) as reported in [52,53], where the shift of the BEs to lower values is assigned to the formation of bigger size NPs.

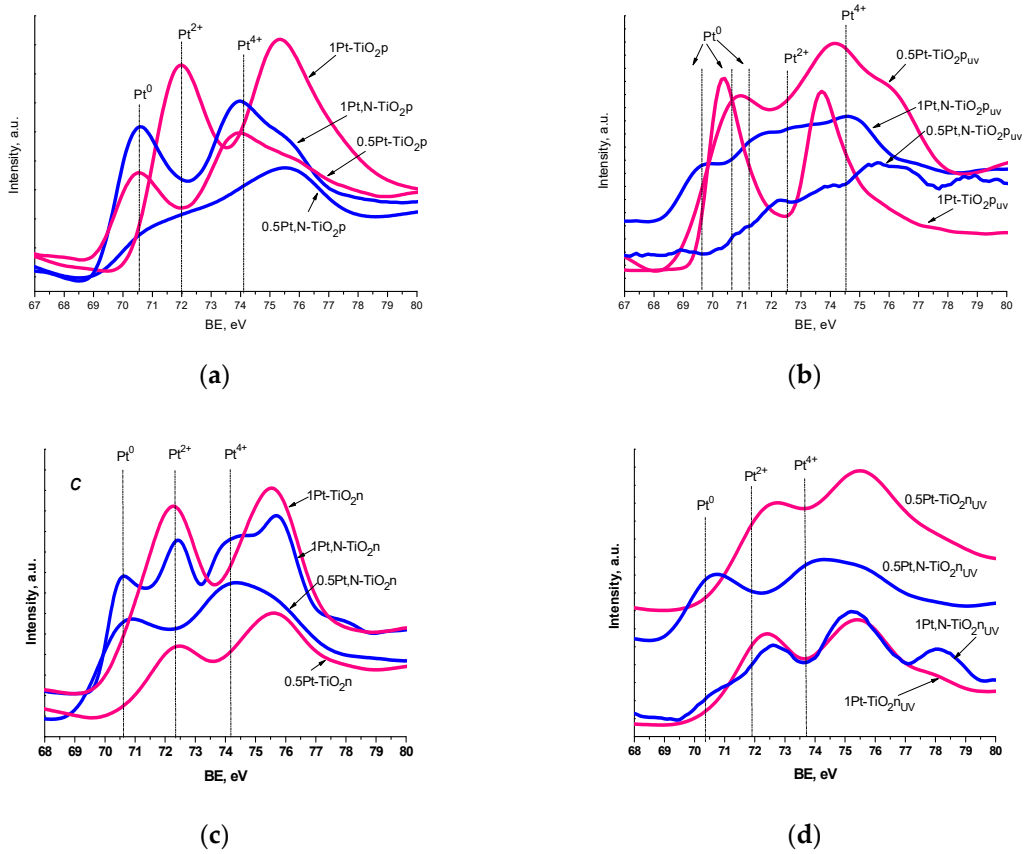

Figure 6. Pt4f XPS spectra of the films: (**a**,**b**) Method 1 and (**c**,**d**) Method 2 without (**a**,**c**) and with (**b**,**d**) UV pretreatment.

Table 4. The position of XPS deconvoluted Pt4f peaks and their relative intensity.

BE, eV	Pt^0		Pt^{2+}		Pt^0		Pt^{2+}		Pt^{4+}	
	$Pt4f_{7/2}$	I_{rel}	$Pt4f_{7/2}$	I_{rel}	$Pt4f_{7/2}$	I_{rel}	$Pt4f_{7/2}$	I_{rel}	$Pt4f_{7/2}$	I_{rel}
Film			***Method 1***				***Method 2***			
0.5Pt-TiO_2	70.2	51.2	71.0 72.4	36.3 12.5	-	-	72.3	100.0		
0.5Pt,N-TiO_2	70.8	48.3	72.4	51.7	70.6	56.3	72.3	43.7	-	-
0.5Pt-TiO_{2UV}	70.7	62.3	72.5	37.7	-	-	72.4	85.3	74.2	14.7
0.5Pt,N-TiO_{2UV}	71.0	32.5	72.1	67.5	70.6	69.5	72.3	30.5	-	-
1Pt-TiO_2	71.4	11.6	72.1	88.4	-	-	72.0	100.0	-	-
1Pt,N-TiO_2	70.4	76.6	72.0	23.4	70.5	19.5	71.2 72.5	29.2 45.5	74.3	5.8
1Pt-TiO_{2UV}	70.3	55.5	71.1	44.5	-	-	72.3	83.8	74.3	16.2
1Pt,N-TiO_{2UV}	69.6	40.2	71.4	59.8	70.8	15.2	72.5	55.9	74.6	28.9

It has to be noted that Pt^0 is fixed for all the films of Method 1 and some of Method 2, as shown by the deconvoluted XPS Pt4f region (examples of spectra are in Figure 7). In the case of Method 1 samples, the reduction process can be caused by the presence of high-molecular weight organic components in the formed sol (Pluronic 123, acetylacetone). No Pt^0 is observed for the Pt-doped films

of Method 2 obtained from the sol containing low-molecular weight organic compounds (iso-propanol). Nevertheless, an effect of urea on Pt^{2+} reduction is pronounced for the nitrogen-containing films of Method 2. A likely possibility is that an intermediate of urea decomposition, ammonium cyanate [50], formed during thermal treatment, plays the role of a reducing agent in this process. As evidence, the oxidative forms of nitrogen are detected in N1s spectra in the range of 400.5–404.1 eV.

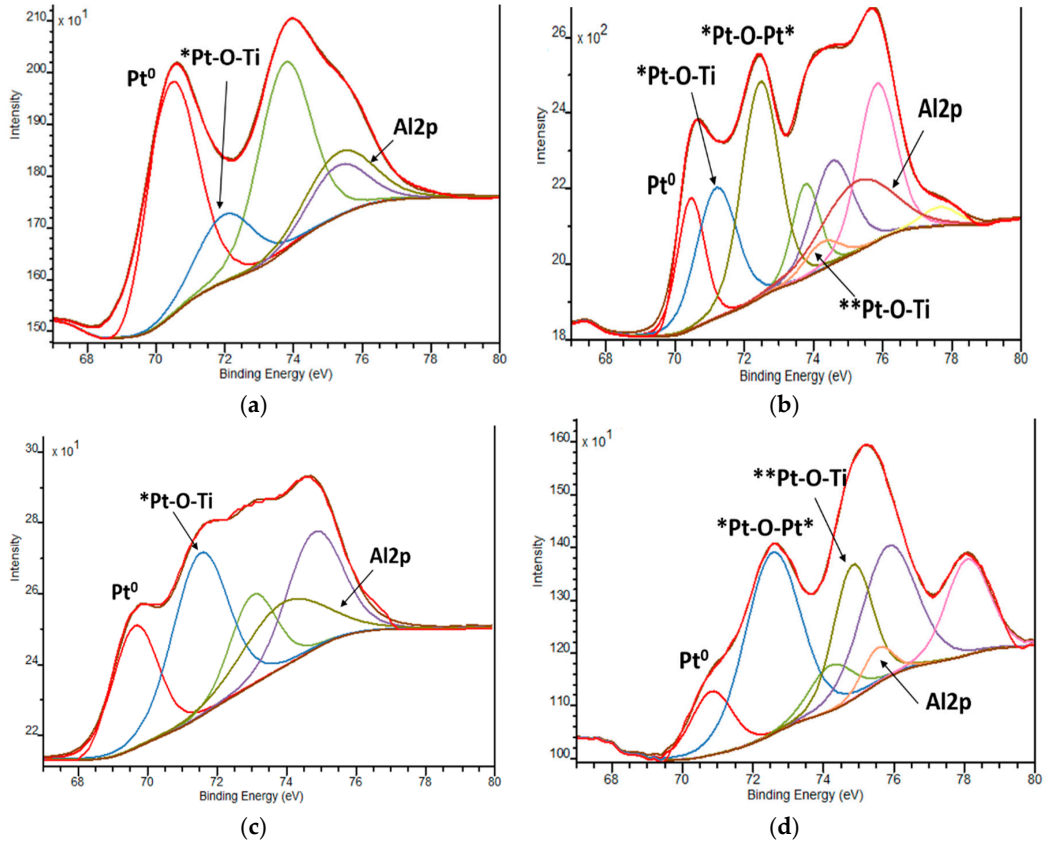

Figure 7. Deconvoluted Pt4f XPS spectra: (**a**) 1Pt,N-TiO_{2M1}; (**b**)1Pt,N-TiO_{2M2}; (**c**) 1Pt,N-TiO_{2M1UV}; (**d**) 1Pt,N-TiO_{2M2UV}. Pt^0, *Pt and **Pt are related to Pt in 0, +2 and +4 oxidation states, respectively.

The positions of $Pt4f_{7/2}$ ascribed to PtO and PtO_2 are stated at 72.4 and 74.9 eV, respectively. The deviations of the $Pt4f_{7/2}$ BE values from the standard ones are observed in our case. The maxima of deconvoluted $Pt4f_{7/2}$ lines at 71.1–72.1 eV and 74.2–74.6 eV are ascribed to Pt^{2+} and Pt^{4+} ions surrounded by Ti as a less electronegative element than Pt in PtO and PtO_2 structures, respectively, suggesting the most probable formed fragments are Pt-O-Ti. BE values at 72.3–72.5 eV are assigned to the formation of Pt-O-Pt bonds with the +2 oxidation state of Pt.

It has to be mentioned that the oxidation of Pt^{2+} to Pt^{4+} ions takes place only in the case of the films of Method 2, independently of nitrogen doping. The oxidation of Pt^{2+} ions can be caused by the thermal decomposition of $Pt(acac)_2$ under certain conditions [54,55].

EDS mapping and TEM images (Figure 8) confirm the formation of Pt NPs in the structures of the films of Method 1. In the case of Method 2, no Pt^0 NPs are observed for 1Pt-TiO_2n while an additional map scanning at a higher magnification shows rare Pt^0 NP's for 1Pt,N-TiO_{2M2}.

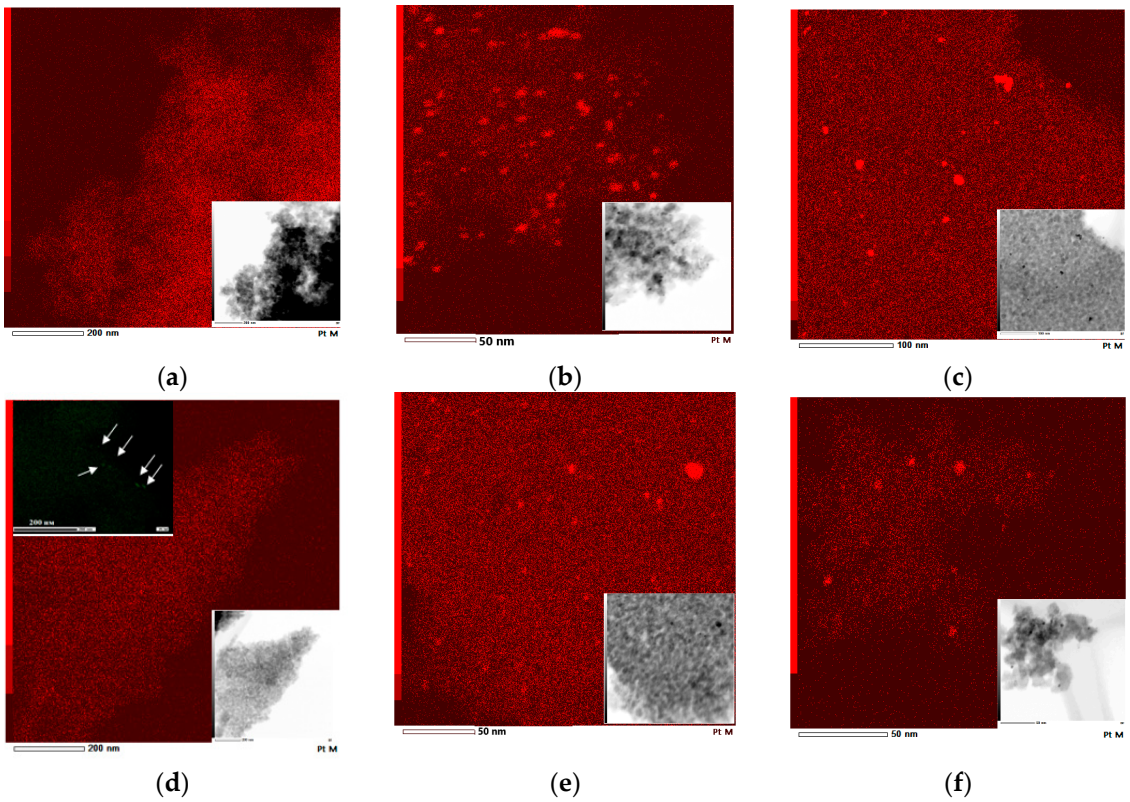

Figure 8. EDS mapping for Pt element and corresponding TEM images (insert): (**a**) 1% Pt-TiO_{2M2}; (**b**) 1% Pt-TiO_{2M1}; (**c**) 1% Pt-TiO_{2M1UV}; (**d**) 1% Pt,N-TiO_{2M2}; (**e**) 1% Pt,N-TiO_{2M1}; (**f**) 1% Pt,N-TiO_{2M1UV}. An additional insert presents EDS mapping for Pt at higher magnification.

The mean sizes of the TiO_2 and Pt^0 obtained from TEM images (Figure 9) and summarized in Table 5 point out a nanoparticle formation in the range of 9–14 nm and 3–4 nm, respectively. No significant size difference is observed for the films synthesized under different conditions, except for 1% Pt-N-TiO_{2M1UV} film. The formation of larger Pt NPs can be explained by the appearance of the initial Pt crystallization centers due to UV treatment. A more even distribution of the nanoparticles was observed for the samples doped only with platinum. No Pt NPs were observed for the 1% Pt-TiO_{2M2} sample. The electron diffraction patterns (Figure S6) of the samples prove the formation of polycrystalline TiO_2. The observed interplanar distance between adjacent planes (d-spacing) of the single crystals (Table 5) corresponds to the anatase (1 0 1) polymorph of TiO_2.

The correlation of the photocatalytic activity of the films in the TC degradation process vs. the Pt oxidation states/atomic contents and atomic nitrogen content is presented in Figure 10. For this purpose, the relative atomic contents (RACs) of Pt species (Table 6) have been obtained by the recalculation of the total Pt atomic contents (the ratios of the elements are presented in Table 2) and the relative intensities were previously presented in Table 4.

Comparing the photocatalytic activity of Method 1 materials (Figure 10a), one can note that the films synthesized using 1 mol.% $Pt(acac)_2$ exhibit a higher conversion of TC molecules. It is also obvious that RACs of Pt species affect the photoperformance of the photocatalysts: the higher the RAC of Pt^0 is, the lower the TC conversion that occurs. In cases of a low RAC of Pt^{2+}, the presence of nitrogen seems to be crucial for an increased activity. The low photoactivity of 0.5Pt-TiO_{2M1UV} and 0.5Pt,N-TiO_{2M1UV} is explained by the lowest atomic contents of the doping agents among tested materials. As seen from Figure 10a, the presence of urea and UV pretreatment affects the relative atomic content of Pt^0 NPs [46]. Hence, the activity of Pt-containing films of Method 1 can be caused by some mutual parameters: efficient incorporation of Pt^{2+} in the TiO_2 lattice, the low content of Pt^0 and doping by nitrogen.

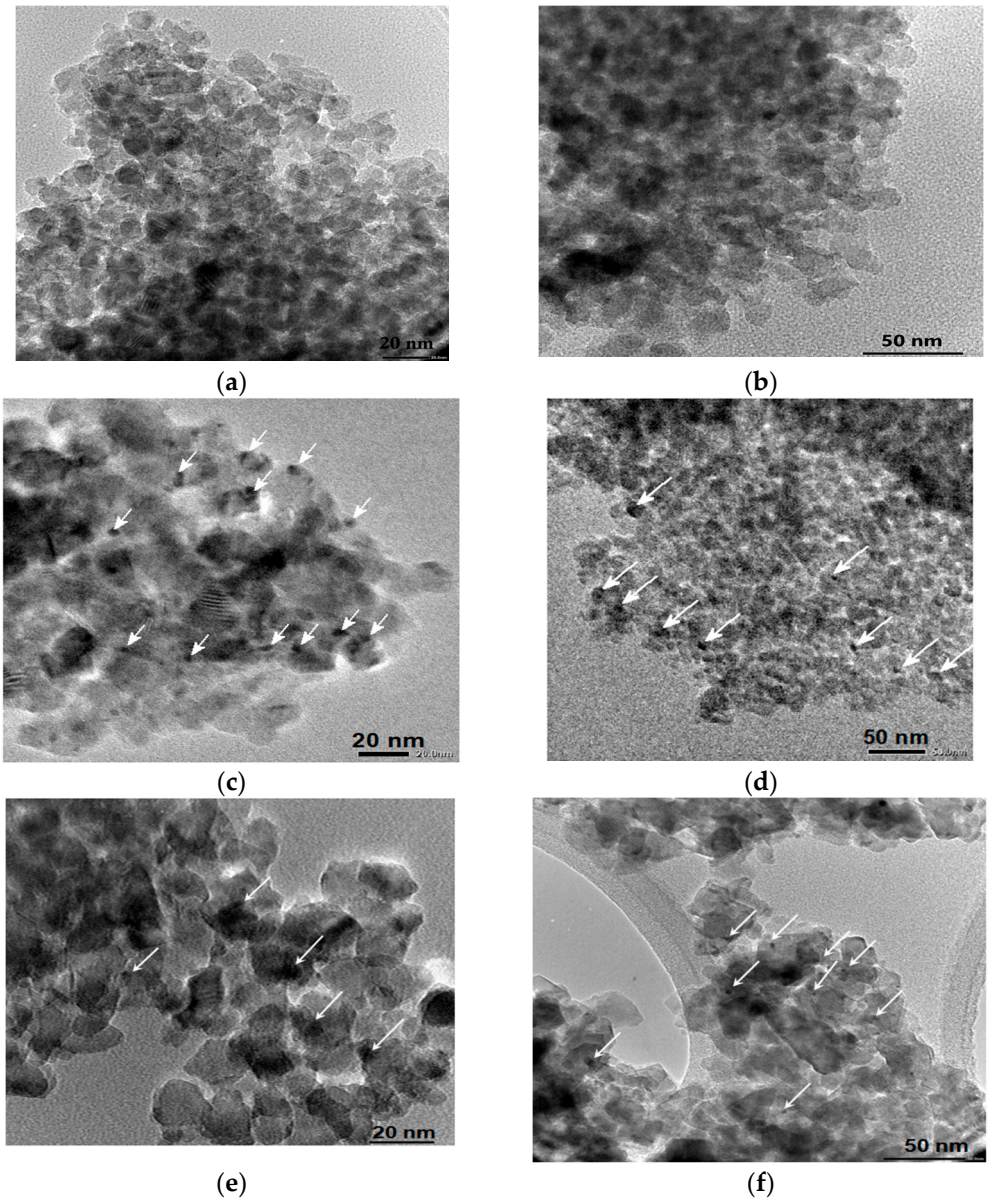

Figure 9. TEM images and electron diffraction patterns: (**a**) 1% Pt-TiO_{2M2}; (**b**) 1% Pt,N-TiO_{2M2}; (**c**) 1% Pt-TiO_{2M1}; (**d**) 1% Pt,N-TiO_{2M1}; (**e**) 1% Pt-TiO_{2M1UV}; (**f**) 1% Pt-N-TiO_{2M1UV}. Pt^0 nanoparticles (NPs) are indicated by the arrows.

Table 5. Mean particle sizes and d-spacing obtained from TEM.

Sample	Mean Particle Size, nm		d-Spacing, nm
	Pt	TiO_2	
1% Pt-TiO_{2M2}	-	8.7 ± 2.6	0.347
1% Pt,N-TiO_{2M2}	3.2 ± 1.5	11.6 ± 1.4	0.351
1% Pt-TiO_{2M1}	3.2 ± 0.8	12.6 ± 1.9	0.350
1% Pt,N-TiO_{2M1}	3.3 ± 0.4	8.7 ± 1.2	0.350
1% Pt-TiO_{2M1UV}	3.2 ± 1.7	11.5 ± 2.1	0.361
1% Pt,N-TiO_{2M1UV}	4.1 ± 2.7	14.1 ± 3.1	0.357

Table 6. Atomic contents (ACs) of N and Pt obtained from XPS data and recalculated relative atomic contents (RACs) of Pt species.

Film	N	Pt	Pt^0	Pt^{2+}	N	Pt	Pt^0	Pt^{2+}	Pt^{4+}
	AC, %		RAC·10^2, %		AC, %		RAC·10^2, %		
	Method 1				*Method 2*				
0.5Pt-TiO_2	-	0.13	6.7	6.3	-	0.18	-	18.0	-
0.5Pt,N-TiO_2	0.51	0.12	5.8	6.2	1.00	0.11	6.2	4.8	-
0.5Pt-TiO_{2UV}	-	0.09	5.6	3.4	-	0.19	-	16.2	2.8
0.5Pt,N-TiO_{2UV}	0.09	0.02	0.7	1.6	0.87	0.19	13.2	5.8	-
1Pt-TiO_2	-	0.13	1.5	11.5	-	0.40	-	40.0	-
1Pt,N-TiO_2	0.26	0.16	12.3	3.7	1.37	0.35	6.8	26.1	2.0
1Pt-TiO_{2UV}	-	0.30	16.7	13.4	-	0.45	-	37.5	7.3
1Pt,N-TiO_{2UV}	0.64	0.11	4.4	6.6	0.90	0.20	3.0	11.0	6.0

Contrary to the films of Method 1, the highest photoactivity of the films of Method 2 (Figure 10b) was observed for nitrogen-doped structures, independently of the molar percentages of $Pt(acac)_2$ loaded during synthesis—the most active films are 0.5Pt,N-TiO_{2M2} and 1Pt,N-TiO_{2M2}, containing the highest N atomic concentrations. The lowest activity of the nitrogen-free film containing only Pt^{2+} ions, 0.5Pt-TiO_{2M2} and 1Pt-TiO_{2M2}, could be caused by ineffective light absorption due to the widest bandgaps among non-porous films (Table 1). One more piece of evidence that can affect the efficiency of photoinduced charge separation is the presence of Pt^{4+} ions that can be additional traps for photogenerated electrons.

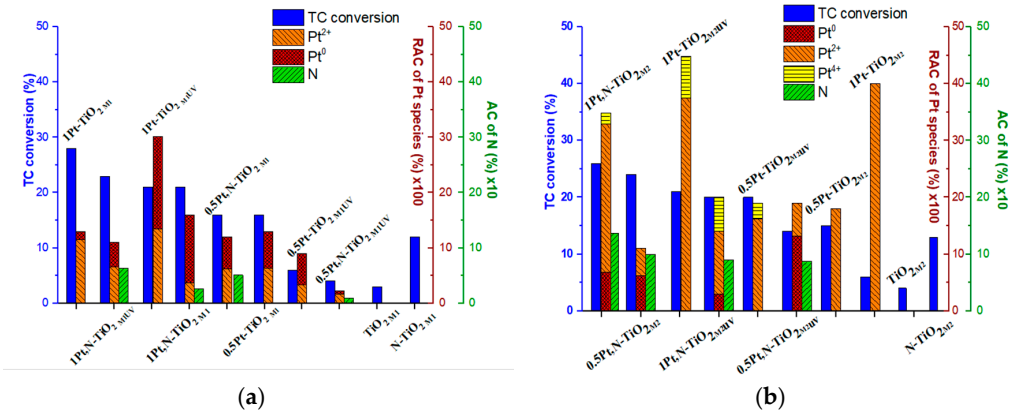

(**a**) (**b**)

Figure 10. Photocatalytic activity of Pt-doped and Pt,N co-doped TiO_2, TiO_2 and N-TiO_2 films obtained by (**a**) Method 1 and (**b**) Method 2 vs. relative atomic content (RAC) of Pt^0 and Pt ions(100) vs. atomic content (AC) of N (10).

3. Discussion

The semiconductor films were obtained by sol-gel methods using different approaches, and their photocatalytic activity was measured by the photodegradation of tetracycline hydrochloride. The enrichment of the film surface of Method 2 by Pt and N as well as the homogeneous distribution of doped metal on the surface and bulk compared to Method 1 was established by XPS and EDS data. The XPS results reveal that nitrogen is mostly presented in C-N-C, O-N-O(C), and Ti-O-N fragments. Nitrogen incorporation in the forms of substitutional and interstitial atoms was realized for 1Pt,N-TiO_{2M1} and 1Pt,N-TiO_{2M2} resulting in co-doping with platinum ions of titania synthesized by the sol-gel method. The reduction and oxidation of Pt^{2+} to Pt^0 and Pt^{4+} can be achieved owing to the following reaction conditions: doping with urea, presence of some organic components, and UV pretreatment. Depending on the synthesis route, the optical properties are varied: a decrease in bandgap energy values is observed for the films obtained by Method 2 and no influence of nitrogen

and platinum doping is noted for Method 1; the light scattering observed in the absorption spectra of the films obtained by Method 2 is attributed to the saturation of the film surface by Pt^0 NPs.

Taking into account that the TC conversion percentage over TiO_2 and N-TiO_2 films, synthesized in the same manner as platinum-doped films, which is found to be 3–4% and 12–13%, respectively, most of the modified films showed much higher photocatalytic activities, suggesting that Pt species are responsible for the increased photocatalytic degradation as well as visible light absorption. The photocatalytic destruction of tetracycline hydrochloride monitored under a simulated solar light is increased over the samples containing a sufficient amount of Pt^{2+} ions as well as N on their surface, while the increased content of Pt^0 delays their photoactivity. The most active films are 1Pt-TiO_{2M1} (27%) and 1Pt,N-TiO_{2M2} (26%), leading to the conclusion that the morphology of the surface has no effect on the photocatalytic degradation of TC molecules over Pt-doped TiO_2 films, as opposed to the oxidation states, atomic contents and the ratio of platinum and nitrogen species in the surface layer. The proposed mechanism of primary photocatalytic pathways is depicted in Scheme 2. The formation of Pt sublevels under the conduction band of titania responsible for the visible light absorption is suggested. A photogenerated electron can be trapped by Pt^{n+} ions or Pt^0 preventing the recombination process. There is a high probability that these pathways are competitive depending on Pt NPs distribution and content on the surface. It is reported [33] that platinized TiO_2 exhibits a higher photocatalytic activity in the photocatalytic degradation of trichloroethylene, perchloroethylene, dichloroacetate than the sample doped with Pt^{2+}/Pt^{4+} ions. On the other hand, the increased Pt loading to 1% causes a decrease in the reaction rate of methanol formation over platinized TiO_2 samples [27]. It is suggested that the decrease in photoactivity of the materials takes place due to (i) the narrowing of the space charge layer with higher Pt loading leading to the deeper penetration depth of light resulting in the favorable electron-hole recombination and/or (ii) the light screening by Pt^0 particles causing the less effective electron-hole pair formation.

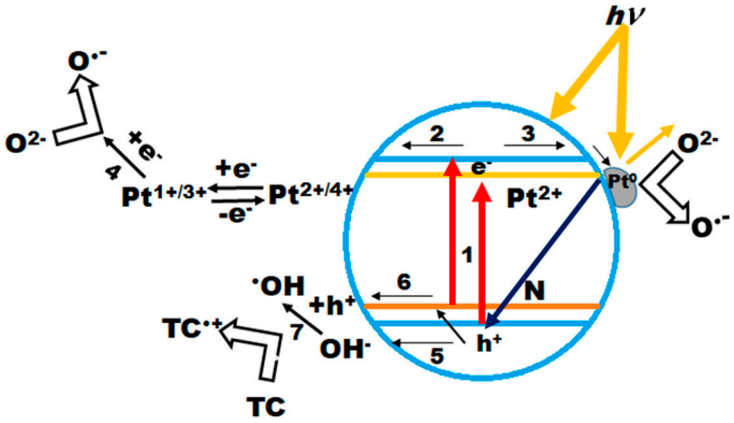

Scheme 2. Proposed mechanism of the primary photocatalytic steps on the surface of Pt(N)-TiO_2 films.

After light absorption with energy lower (the lines in the spectrum of the used lamp with a cut-off filter shown in Figure S1 are 364, 404 and 434 nm corresponding to 3.4, 3.1 and 2.9 eV, respectively) than the bandgap energy of titania (step 1), the transition of an electron from the valence band to the sublevel of Pt or from the N sublevel to the conduction band can occur. It appears that Pt ions play the role of trapping centers for photogenerated electrons, with a following reduction in oxygen molecules to superoxide radicals, and Pt oxidation to its previous oxidation state (steps 2 and 4) [25]. As shown by the experimental results, the higher content of Pt^0 has a detrimental effect on photocatalytic processes, suggesting their light screening from the TiO_2 surface or preferential charge recombination, as proposed in [27]. The oxidation pathways are strongly dependent on the trapping efficiency of photoformed electrons and a consequence can be the direct interaction of h^+ with surface OH groups or via the trapping by N species, in the case of N-containing materials (steps 5 and 6). The resulting OH radical oxidizes the TC molecule (step 7). It is most probable that the nitrogen species are able to

prevent the charge recombination by trapping a hole, which is confirmed by the high photoreactivity of the nitrogen-doped films of Method 2. Thus, the design of materials with controlled oxidation states of Pt and N in TiO_2 is a prospective strategy to drive the development of solar photocatalysts.

4. Materials and Methods

The platinum and nitrogen co-doped titania films were synthesized by sol-gel techniques using two different procedures. To obtain porous films, the sols containing the alcoholic (iso-propanol, Reider-de-Haën) solution of titanium tetraisopropoxide (TTIP, Merk, Darmstadt, Germany), three-block copolymer of polyethyleneoxide and polypropyleneoxide $(PEO)_{20}(PPO)_{70}(PEO)_{20}$ (Pluronic 123, Sigma-Aldrich, Schnelldorf, Germany) and acetylacetone (acac, Sigma-Aldrich) were used. Platinum (II) acetylacetonate ($Pt(acac)_2$, ACROS, 98%) (0.5 or 1.0 mol.%) dissolved in acetone and urea (5% mol., Sigma-Aldrich) dissolved in ethanol (SC Chimreactiv SRL) were added to the sol as the doping agents. The molar ratio of the main components in the sols was established as Ti(O*i*-Pr)$_4$:P123:acac:C_3H_6O:C_3H_7OH:$HClO_4$:0.5(1)mol.% $Pt(acac)_2$:$(NH_2)_2CO$ = 1.0:0.05:0.5:5.4(8.2):26.4:0.3:0.005(0.01):0.05. The films were signed as xPt(N)-TiO_{2M1}, where x is the molar percentage of $Pt(acac)_2$ and M1 means Method 1. The synthesis of non-porous films has been performed using the preliminary cold and acidified (concentrated $HClO_4$, Sigma-Aldrich) mixture of iso-propanol, $Pt(acac)_2$ in acetone and ethanol solution of urea (in the case of nitrogen-doped films) with the following dropwise addition of an appropriate amount of TTIP under continuous stirring. The molar ratio of the components in the resulting sol was TTIP:0.5(1)mol.% $Pt(acac)_2$:C_3H_6O:C_3H_7OH:$HClO_4$:$(NH_2)_2CO$ = 1:0.005(0.01):2.4:16.2:0.02:0.05 (xPt(N)-TiO_{2M2}, where M2—Method 2). Nitrogen-free Pt-doped materials have been synthesized according to the above-mentioned routes without adding urea. For both procedures, the three-layered films have been obtained by a dip-coating procedure at a withdrawal rate of 1.5 mm/s. A glass slide (Microscope Slides Cat.No. 7102, Zhejiang, China, in the size of 25.4 × 76.2 mm) was used as a substrate for the synthesis of the films. The different pretreatments between the layers have been performed: hydrolysis for 30 min in the presence of air with the following heating of the first two layers at 200 °C for 10 min (xPt(,N)-TiO_2n and xPt(,N)-TiO_2p) or heating of the first two layers at 200 °C for 10 min and UV treatment (1000 W middle-pressure mercury lamp) for 30 sec (xPt(,N)-TiO_2n_{UV} and xPt(,N)-TiO_2p_{UV}). After hydrolysis (1h) of the last third layer, the thermal treatment of the films was performed at 450 °C for 20 min at the heating rate of 7 °C/min in the presence of air. The porous and non-porous pure TiO_2 and N-doped TiO_2 films were obtained in the same manner as Pt-doped ones without adding a solution of $Pt(acac)_2$ in acetone. No UV pretreatment was performed for these films.

Absorption spectra of the films were recorded with a double beam spectrophotometer (Lambda 35, PerkinElmer) within the wavelength range of 190–1200 nm. The bandgap energy values of doped TiO_2 films were determined according to the modified Tauc method reported in [56]. XRD patterns of the films scratched off from the glass were performed on DRON-4-07 using Cu Kα irradiation (λ = 1.5418 Å). The anatase crystallite size was calculated using the Scherrer equation and was about 14 nm for all Pt-doped films. The surface morphology of the films was monitored by scanning electron microscopy (SEM) using an FEI Inspect S Scanning Electron Microscope at an acceleration voltage of 20kV, in a high vacuum. The samples were coated with a thin Au film. XPS measurements were carried out with an ESCALAB Xi$^+$ (Thermo SCIENTIFIC Surface Analysis, Thermo Fisher Scientific, UK) setup equipped with a multichannel hemispherical electron Analyzer (dual X-ray source) working with Al Kα radiation ($h\nu$ = 1486.2 eV), using C 1s (284.8 eV) as the energy reference. XPS data were recorded on samples that had been outgassed in the prechamber of the instrument at room temperature at a pressure of $<2 \times 10^{-8}$ Pa to remove chemisorbed water from their surfaces. The surface chemical composition and oxidation state were estimated from XPS spectra by calculating the integral of each peak after a subtraction of the "S-shaped" Shirley-type background. The spectra were fitted with CasaXPS software (Casa Software Ltd, Teignmouth, United Kingdom) using the appropriate experimental sensitivity factors. Structural features of films have been studied with high resolution transmission electron microscopy (TEM)

imaging on an analytical JEOL JEM-2800 (JEOL Ltd., Tokyo, Japan) with an accelerating voltage of 200 kV. Samples were allocated on copper grids with lacey carbon film by drop-casting, using ethanol as a transferring agent, after having been scratched from a glass substrate samples using a scalpel. The mean particle size was calculated from HR-TEM images using 30–50 particles. Electron diffraction patterns were acquired by selected area diffraction, and elemental maps were recorded with a large angle high-speed energy dispersive spectrometer (EDS) with an energy resolution of 133.0 eV.

Photocatalytic activity of the films was tested via the degradation of 2×10^{-5} mol/L TC aqueous solution. The change in TC concentration was monitored with a Lambda 35 UV–vis spectrophotometer (PerkinElmer, Norwalk, USA) every 20 min; the conversion percentage was calculated from the change in the absorption intensity at $\lambda = 357$ nm. Prior to photocatalytic reactions, the adsorption equilibrium of the film-liquid system was reached by stirring in the dark. A system (a quartz reactor filled with 40 mL of 2×10^{-5} mol/L TC and a film under constant stirring and reaction temperature of 25 °C) was irradiated with a 1000 W middle-pressure mercury lamp with the corresponding cut-off filter (Figure S1c, spectrum 2) for 90 min. The distance lamp reactor was set at 90 cm. Two blank experiments, the catalytic reaction (under dark conditions in the presence of a film) and the photolysis of TC (without photocatalyst), showed no significant changes in TC absorption spectra. The most active films, 1Pt-TiO_2p and 1Pt,N-TiO_2n, have been thricely tested for the repeatability of their photocatalytic performance resulting in ±5% variation of TC conversion.

Supplementary Materials: The following are available online at http://www.mdpi.com/2073-4344/10/9/1074/s1, Figure S1: Absorption spectra of the films obtained by *Method 1* (a) and *Method 2* (b), Figure S2: Tauc plots of the films obtained by *Method 1* (a) and *Method 2* (b) TiO_2 (1) and N-TiO_2 (2) films, Figure S3: XRD patterns of N-TiO_2 films obtained by *Method 1* (1) and *Method 2* (2): a-anatase and b-brookite, Figure S4: N1s, Ti2p and O1s XPS spectra of the N-TiO_2 films obtained by *Method 1* (left) and *Method 2* (right), Figure S5: Deconvoluted XPS O1s spectra of Pt and Pt,N co-doped titania films, Figure S6: (a) 1%Pt-TiO_{2M2}; (b) 1%Pt-TiO_{2M1}; (c) 1%Pt-TiO_{2M1UV}; (d) 1%Pt,N-TiO_{2M2}; (e) 1%Pt,N-TiO_{2M1}; (f) 1%Pt,N-TiO_{2M1UV}, Table S1: Binding energy values of Pt4f XPS spectra.

Author Contributions: Conceptualization, O.L.; validation, D.I., C.T., O.L. and I.T.; formal analysis, D.I., C.T., O.L. and I.T.; investigation, D.I., C.T. and O.L.; writing—original draft preparation, O.L.; writing—review and editing, D.I., C.T., O.L. and I.T.; visualization, D.I., C.T. and O.L.; funding acquisition, I.T. All authors have read and agreed to the published version of the manuscript.

Funding: This research was partially funded by Academy of Finland, grant numbers 285972 and 319018.

Acknowledgments: The authors thankfully acknowledge C. Mihailescu and G. Popescu-Pelin from the National Institute for Lasers, Plasma and Radiation Physics, Romania for XPS and SEM measurements. Part of the research presented in this paper was conducted at the Micronova microfabrication center and at the Nanomicroscopy Center, both part of the OtaNano research infrastructure in Aalto University. C.T. acknowledges the financial support of the Vilho, Yriö ja Kalle Väisälä Fund issued by the Finnish Academy of Sciences and Letters. C.T. and I.T. acknowledge the financial support of the Academy of Finland, projects 285972 and 319018, and the Academy of Finland Flagship Programme PREIN (320167).

Conflicts of Interest: The authors declare no conflict of interest.

References

1. Kutsenko, V.Y.; Lopatina, Y.Y.; Bossard-Giannesini, L.; Marchenko, O.A.; Pluchery, O.; Snegir, S.V. Alkylthiol self-assembled monolayers on Au(111) with tailored tail groups for attaching gold nanoparticles. *Nanotechnology* **2017**, *28*, 1–8. [CrossRef] [PubMed]
2. Ischenko, E.V.; Yatsimirsky, V.K.; Dyachenko, A.G.; Borysenko, M.V. Cu-Co-Fe oxide catalysts supported on carbon nanotubes in the reaction of CO oxidation. *Pol. J. Chem.* **2008**, *82*, 291–297.
3. Laguta, I.; Stavinskaya, O.; Kazakova, O.; Fesenko, T.; Brychka, S. Green synthesis of silver nanoparticles using Stevia leaves extracts. *Appl. Nanosci.* **2019**, *9*, 755–765. [CrossRef]
4. Vareda, J.P.; Valente, A.J.M.; Duraes, L. Assessment of heavy metal pollution from anthropogenic activities and remediation strategies: A review. *J. Environ. Manag.* **2019**, *246*, 101–118. [CrossRef]
5. Etacheri, V.; Di Valentin, C.; Schneider, J.; Bahnemann, D.; Pillai, S.C. Visible-light activation of TiO_2 photocatalysts: Advances in theory and experiments. *J. Photochem. Photobiol. C* **2015**, *25*, 1–29. [CrossRef]
6. Mitoraj, D.; Kisch, H. The nature of nitrogen-modified titanium dioxide Photocatalysts active in visible light. *Angew. Chem. Int. Ed.* **2008**, *47*, 9975–9978. [CrossRef]

7. Surówka, M.; Kobielusz, M.; Trochowski, M.; Buchalska, M.; Kruczała, K.; Broś, P.; Macyk, W. Iron and other metal species as phase-composition controllers influencing the photocatalytic activity of TiO_2 materials. *Appl. Catal. B: Environ.* **2019**, *247*, 173–181. [CrossRef]
8. Linnik, O.; Chorna, N.; Smirnova, N. Nonporous iron titanate thin films doped with nitrogen: Optical, structural and photocatalytic properties. *Nanoscale Res. Lett.* **2017**, *12*, 249–258. [CrossRef]
9. Dolat, D.; Mozia, S.; Ohtani, B.; Morawski, A.W. Nitrogen, iron-single modified (N-TiO_2, Fe-TiO_2) and co-modified (Fe,N-TiO_2) rutile titanium dioxide as visible-light active photocatalysts. *Chem. Eng. J.* **2013**, *225*, 358–364. [CrossRef]
10. Chorna, N.; Smirnova, N.; Vorobets, V.; Kolbasov, G.; Linnik, O. Nitrogen doped iron titanate films: Photoelectrochemical, electrocatalytic, photocatalytic and structural features. *Appl. Surf. Sci.* **2019**, *473*, 343–351. [CrossRef]
11. Kisch, H. *Semiconductor Photocatalysis Principles and Application*; Wiley-VCH Verlag GmbH&Co: Weinheim, Germany, 2015; pp. 55–68. [CrossRef]
12. Sato, S. Photocatalytic activity of NOx-doped in the visible light region. *Chem. Phys. Lett.* **1986**, *123*, 126–128. [CrossRef]
13. Asahi, R.; Morikawa, T.; Ohwaki, T.; Aoki, K.; Taga, Y. Visible-light photocatalysis in nitrogen-doped titanium oxides. *Science* **2001**, *293*, 269–271. [CrossRef] [PubMed]
14. Socol, G.; Gnatyuk, Y.; Stefan, N.; Smirnova, N.; Djokić, V.; Sutan, C.; Malinovschi, V.; Stanculescu, A.; Korduban, O.; Mihailescu, I.N. Photocatalytic activity of pulsed laser deposited TiO_2 thin films in N_2, O_2 and CH_4. *Thin Solid Films* **2010**, *518*, 4648–4653. [CrossRef]
15. Sakthivel, S.; Janczarek, M.; Kisch, H. Visible light activity and photoelectrochemical properties of nitrogen-doped TiO_2. *J. Phys. Chem. B* **2004**, *108*, 19384–19387. [CrossRef]
16. Tryba, B.; Wozniak, M.; Zolnierkiewicz, G.; Guskos, N.; Morawski, M.; Colbeau-Justin, C.; Wrobel, R.; Nitta, A.; Ohtani, B. Influence of an electronic structure of N-TiO_2 on its photocatalytic activity towards decomposition of acetaldehyde under UV and fluorescent lamps irradiation. *Catalysts* **2018**, *8*, 85. [CrossRef]
17. Sirivallop, A.; Areerob, T.; Chiarakorn, S. Enhanced visible light photocatalytic activity of N and Ag doped and co-doped TiO_2 synthesized by using an in-situ solvothermal method for gas phase ammonia removal. *Catalysts* **2020**, *10*, 251. [CrossRef]
18. Somekawa, S.; Kusumoto, Y.; Ikeda, M.; Ahmmad, B.; Horie, Y. Fabrication of N-doped TiO_2 thin films by laser ablation method: Mechanism of N-doping and evaluation of the thin films. *Catal. Commun.* **2008**, *9*, 437–440. [CrossRef]
19. Pandian, R.; Natarajan, G.; Dhaipule, K.N.G.; Prasad, A.K.; Kamruddin, M.; Tyagi, A.K. Types of nitrogen incorporation in reactively sputtered titania thin films: Influence on UV–visible, photocatalytic and photoconduction properties. *Thin Solid Films* **2016**, *616*, 466–476. [CrossRef]
20. Saha, N.C.; Tompkins, H.G. Titanium nitride oxidation chemistry: An x-ray photoelectron spectroscopy study. *J. Appl. Phys.* **1992**, *72*, 3072–3079. [CrossRef]
21. Asahi, R.; Morikawa, T. Nitrogen complex species and its chemical nature in TiO_2 for visible-light sensitized photocatalysis. *Chem. Phys.* **2007**, *339*, 57–63. [CrossRef]
22. Di Valentin, C.; Pacchioni, G.; Selloni, A.; Livraghi, S.; Giamello, E. Characterization of paramagnetic species in N-doped TiO_2 powders by EPR spectroscopy and DFT calculations. *J. Phys. Chem. B* **2005**, *109*, 11414–11419. [CrossRef] [PubMed]
23. Napoli, F.; Chiesa, M.; Livraghi, S.; Giamello, E.; Agnoli, S.; Granozzi, G.; Pacchioni, G.; Di Valentin, C. The nitrogen photoactive centre in N-doped titanium dioxide formed via interaction of N atoms with the solid. Nature and energy level of the species. *Chem. Phys. Lett.* **2009**, *477*, 135–138. [CrossRef]
24. Wu, M.; Hiltunen, J.; Sápi, A.; Avila, A.; Larsson, W.; Liao, H.; Huuhtanen, M.; Tóth, G.; Shchukarev, A.; Laufer, N.; et al. Nitrogen-doped anatase nanofibers decorated with noble metal nanoparticles for photocatalytic production of hydrogen. *ACS Nano* **2011**, *5*, 5025–5030. [CrossRef]
25. Wang, S.; Ding, Z.; Chang, X.; Xu, J.; Wang, D.-H. Modified nano-TiO_2 based composites for environmental photocatalytic applications. *Catalysts* **2020**, *10*, 759. [CrossRef]
26. Linnik, O.; Smirnova, N.; Korduban, O.; Eremenko, A. Gold nanoparticles into $Ti_{1-x}Zn_xO_2$ films: Synthesis, structure and application. *Mater. Chem. Phys.* **2013**, *142*, 318–324. [CrossRef]

27. Ahmed, L.M.; Ivanova, I.; Hussein, F.H.; Bahnemann, D.W. Role of platinum deposited on TiO_2 in photocatalytic methanol oxidation and dehydrogenation reactions. *Int. J. Photoenergy* **2014**, *2014*, 1–9. [CrossRef]
28. Kim, S.; Hwang, S.-J.; Choi, W. Visible light active platinum-ion-doped TiO_2 photocatalyst. *J. Phys. Chem. B* **2005**, *109*, 24260–24267. [CrossRef]
29. Guayaquil-Sosa, J.F.; Calzada, A.; Serrano, B.; Escobedo, S.; de Lasa, H. Hydrogen production via water dissociation using Pt–TiO_2 photocatalysts: An oxidation–reduction network. *Catalysts* **2017**, *7*, 324. [CrossRef]
30. Higashimoto, S.; Katsuura, K.; Yamamoto, M.; Takahashi, M. Photocatalytic activity for decomposition of volatile organic compound on Pt-WO_3 enhanced by simple physical mixing with TiO_2. *Catal. Commun.* **2020**, *133*, 105831. [CrossRef]
31. Tossi, C.; Hällström, L.; Selin, J.; Vaelma, M.; See, E.; Lahtinen, J.; Tittonen, I. Size- and density-controlled photodeposition of metallic platinum nanoparticles on titanium dioxide for photocatalytic applications. *J. Mater. Chem. A* **2019**, *7*, 14519–14525. [CrossRef]
32. See, E.M.; Tossi, C.; Hällström, L.; Tittonen, I. Photodeposition of RuO_x nanostructures on TiO_2 films with a controllable morphology. *ACS Omega* **2020**, *5*, 10671–10679. [CrossRef] [PubMed]
33. Lee, J.; Choi, W. Photocatalytic reactivity of surface platinized TiO_2: Substrate specificity and the effect of Pt oxidation state. *J. Phys. Chem. B* **2005**, *109*, 7399–7406. [CrossRef] [PubMed]
34. Sun, H.; Zhou, G.; Liu, S.; Ang, H.M.; Tadé, M.O.; Wang, S. Visible light responsive titania photocatalysts codoped by nitrogen and metal (Fe, Ni, Ag, or Pt) for remediation of aqueous pollutants. *Chem. Eng. J.* **2013**, *231*, 18–25. [CrossRef]
35. Gaponenko, N.V.; Kortov, V.S.; Smirnova, N.P.; Orekhovskaya, T.I.; Nikolaenko, I.A.; Pustovarov, V.A.; Zvonarev, S.V.; Slesarev, A.I.; Linnik, O.P.; Zhukovskii, M.A.; et al. Sol–gel derived structures for optical design and photocatalytic application. *Microelectron. Eng.* **2012**, *90*, 131–137. [CrossRef]
36. Kang, T.D.; Yoon, J.-G. Optical characterization of surface plasmon resonance of Pt nanoparticles in TiO_2-SiO_2 nanocomposite films. *J. Appl. Phys.* **2017**, *122*, 134302. [CrossRef]
37. Beranek, R.; Kisch, H. Tuning the optical and photoelectrochemical properties of surface-modified TiO_2. *Photochem. Photobiol. Sci.* **2008**, *7*, 40–48. [CrossRef]
38. Mitoraj, D.; Kisch, H. On the mechanism of urea-induced titania modification. *Chem. A Eur. J.* **2010**, *16*, 261–269. [CrossRef]
39. Linnik, O.; Khoroshko, L. Non-porous nitrogen and ruthenium co-doped titania films for photocatalysis. *Int. J. Nanosci.* **2019**, *18*, 1940043. [CrossRef]
40. Zhang, Z.; Wang, X.; Long, J.; Gu, Q.; Ding, Z.; Fu, X. Nitrogen-doped titanium dioxide visible light photocatalyst: Spectroscopic identification of photoactive centers. *J. Catal.* **2010**, *276*, 201–214. [CrossRef]
41. Linnik, O.; Petrik, I.; Smirnova, N.; Kandyba, V.; Korduban, O.; Eremenko, A.; Socol, G.; Stefan, N.; Ristoscu, C.; Mihailescu, I.N.; et al. TiO_2/ZrO_2 thin films synthesized by PLD in low pressure N-, C- and/or O-containing gases: Structural, optical and photocatalytic properties. *Dig. J. Nanomater. Biostruct.* **2012**, *7*, 1343–1352.
42. Linnik, O.; Popescu-Pelin, G.; Stefan, N.; Chorna, N.; Smirnova, N.; Mihailescu, C.N.; Ristoscu, C.; Mihailescu, I.N. Investigation of iron doped TiO_2 films synthesized in N_2/CH_4 via pulsed laser deposition technique. *Appl. Nanosci.* **2020**. [CrossRef]
43. Sakatani, Y.; Ando, H.; Okusako, K.; Koike, H. Metal ion and N co-doped TiO_2 as a visible-light photocatalyst. *J. Mater. Res.* **2004**, *19*, 2100–2108. [CrossRef]
44. Hao, H.; Zhang, J. The study of Iron (III) and Nitrogen co-doped mesoporous TiO_2 photocatalysts: Synthesis, characterization and activity. *Microporous Mesoporous Mater.* **2009**, *121*, 52–57. [CrossRef]
45. Bear, J.C.; Gomez, V.; Kefallinos, N.S.; Mcgettrick, J.D.; Barron, A.R.; Dunnill, C.W. Anatase/rutile bi-phasic titanium dioxide nanoparticles for photocatalytic applications enhanced by nitrogen doping and platinum. *J. Colloid Interface Sci.* **2015**, *460*, 29–35. [CrossRef] [PubMed]
46. Batalovic, K.; Bundaleski, N.; Radaković, J.; Abazović, N.; Mitrić, M.; Silva, R.A.; Savić, M.; Belošević-Čavor, J.; Rakočević, Z.; Rangel, C.M. Modification of N-doped TiO_2 photocatalysts using noble Metals (Pt, Pd)—A combined XPS and DFT study. *Phys. Chem. Chem. Phys.* **2017**, *19*, 7062–7071. [CrossRef]
47. Theophanides, T.; Harvey, P.D. Structural and spectroscopic of metal-urea complexes. *Coord. Chem. Rev.* **1987**, *76*, 237–264. [CrossRef]

48. Woon, T.C.; Wickramasinghe, W.A.; Fairlie, D.P. Oxygen versus nitrogen coordination of a urea to (diethylenetriamine)platinum(II). *Inorg. Chem.* **1993**, *32*, 2190–2194. [CrossRef]
49. Li, J.; Yang, X.; Ishigaki, T. Urea coordinated titanium trichloride Ti III $[OC(NH)_2]_6Cl_3$: A single molecular precursor yielding highly visible light responsive TiO_2 nanocrystallites. *J. Phys. Chem. B* **2006**, *110*, 14611–14618. [CrossRef]
50. Schaber, P.M.; Colson, J.; Higgins, S.; Thielen, D.; Anspach, B.; Brauer, J. Thermal decomposition (pyrolysis) of urea in an open reaction vessel. *Thermochim. Acta* **2004**, *424*, 131–142. [CrossRef]
51. Saeid, S.; Kråkström, M.; Tolvanen, P.; Kumar, N.; Eränen, K.; Mikkola, J.-P.; Kronberg, L.; Eklund, P.; Peurla, M.; Aho, A.; et al. Advanced oxidation process for degradation of carbamazepine from aqueous solution: Influence of metal modified microporous, mesoporous catalysts on the ozonation process. *Catalysts* **2020**, *10*, 90. [CrossRef]
52. Garbarino, S.; Pereira, A.; Hamel, C.; Irissou, E.; Chaker, M.; Guay, D. Effect of size on the electrochemical stability of Pt nanoparticles deposited on gold substrate. *J. Phys. Chem. C* **2010**, *114*, 2980–2988. [CrossRef]
53. Mosquera, A.; Horwat, D.; Vazquez, L.; Gutiérrez, A. Thermal decomposition and fractal properties of sputter-deposited platinum oxide thin films. *J. Mater. Res.* **2012**, *27*, 829–836. [CrossRef]
54. Womes, M.; Lynch, J.; Bazin, D.; Le Peltier, F.; Morin, S.; Didillon, B. Interaction between $Pt(acac)_2$ and alumina surfaces studied by XAS. *Catal. Lett.* **2003**, *85*, 25–31. [CrossRef]
55. Filez, M.; Redekop, E.A.; Poelman, H.; Galvita, V.V.; Ramachandran, R.K.; Dendooven, J.; Detavernier, C.; Marin, G.B. Unravelling the formation of Pt−Ga alloyed nanoparticles on calcined Ga-modified hydrotalcites by in situ XAS. *Chem. Mater.* **2014**, *26*, 5936–5949. [CrossRef]
56. Makuła, P.; Pacia, M.; Macyk, W. How to correctly determine the band gap energy of modified semiconductor photocatalysts based on UV−Vis spectra. *J. Phys. Chem. Lett.* **2018**, *9*, 6814–6817. [CrossRef]